International Journal of Heat and Mass Transfer 234 (2024) 126129

Contents lists available at ScienceDirect

International Journal of Heat and Mass Transfer

journal homepage: www.elsevier.com/locate/hmt

Technical note

Thermal fields induced by oscillating laser beams versus non-oscillating equivalent laser beams — A numerical study

Scholte J.L. Bremer [a,*], Ronald G.K.M. Aarts [b], Gert-willem R.B.E. Römer [a]

[a] Chair of Laser Processing, Department of Mechanics of Solids, Surfaces & Systems, Faculty of Engineering Technology, University of Twente, Drienerlolaan 5, 7522NB Enschede, The Netherlands

[b] Chair of Applied Mechanics and Data Analysis, Department of Mechanics of Solids, Surfaces & Systems, Faculty of Engineering Technology, University of Twente, Drienerlolaan 5, 7522NB Enschede, The Netherlands

ARTICLE INFO

Keywords:
Beam shaping
Galvanometer scanner
Thermal simulation

ABSTRACT

In high power laser material processing, like laser transformation hardening, laser welding or laser cladding, tailoring the laser intensity profile is a method to improve stability of the laser material process and/or improve the processing results. A method to tailor the laser intensity profile in real-time is using a Galvanometer Scanner to quickly and iteratively oscillate the focal spot of the laser beam over a predefined path. Due to the oscillating nature of this beam shaping method, the temporal heat input will differ from the temporal heat input by an equivalent non-oscillated laser intensity distribution. Mathematically this equivalent non-oscillated beam profile is the convolution of the laser intensity distribution of the oscillated focal spot and the predefined oscillation path. This work presents simulation results of laser induced thermal fields. The thermal fields induced by oscillated laser beams at different frequencies are compared with the thermal field induced by the equivalent non-oscillated beam. These comparisons show that even at the highest oscillation frequencies the oscillated and equivalent non-oscillated laser beams induce significantly different in temperature fields (e.g. up to 325 K peak temperature difference) and different cooling rates (10^5 K/s and 5500 K/s respectively).

1. Introduction

In various high power laser material processes the laser intensity distribution in the laser-material interaction zone is tailored, also known as beam shaping, to improve process stability and/or processing results. For example, in laser transformation hardening, tailoring the laser intensity profile affects obtained hardness and residual stress distributions in the laser affected volume [1–3]. Tailoring the laser intensity profile is used in laser welding to increase the process window and to adapt the weld seam parameters [4–6]. In laser cladding, using laser beam shaping the microstructure of the deposited material can be controlled and tailored [7–9].

Beam shaping methods can be classified in two categories. That are *static* beam shaping methods, e.g. using laser transport fibers with different cross-sectional shapes of the fiber cores [9,10], Diffractive Optical Elements [4,11], or custom optics [3,7]. The second category, *dynamic* beam shaping methods, allows to dynamically — i.e. during processing — adapt the beam profile. The most common dynamic beam shaping method uses a Galvanometer Scanner [12,13], but recently also other dynamic beam shaping methods became available for high power laser processes, including but not limited to using Multi Plane Light Conversion [14], Deformable Mirrors [6] or Coherent Beam Combining [15].

When using Galvanometer Scanners, a user-defined path is oscillated iteratively by the small focal spot of the laser beam. The oscillation path is generally superposed on a forward speed in the processing direction. This means that a location on the surface of the substrate in the processing area will be illuminated by the laser spot multiple times. When the laser spot passes this location, it will heat up the material in this location, but the material will cool down between consecutive passes of the laser spot. When the oscillation frequency, i.e. the number of times per second the path is scanned, increases, these temperature variations in the material at this location will reduce. Therefore the temperature history in the material in this location will, with increasing oscillation frequency, approach the temperature history as if an equivalent non-oscillated laser beam illuminates this location. The laser intensity profile of this equivalent non-oscillated laser beam is mathematically a convolution between the oscillation path and laser intensity profile of the oscillated focal spot.

When, from a material point of view, a desired laser intensity profile is specified based on desired peak temperatures and cooling rates, this

* Corresponding author.
E-mail address: s.j.l.bremer@utwente.nl (S.J.L. Bremer).

https://doi.org/10.1016/j.ijheatmasstransfer.2024.126129
Received 3 April 2024; Received in revised form 23 July 2024; Accepted 25 August 2024
Available online 31 August 2024

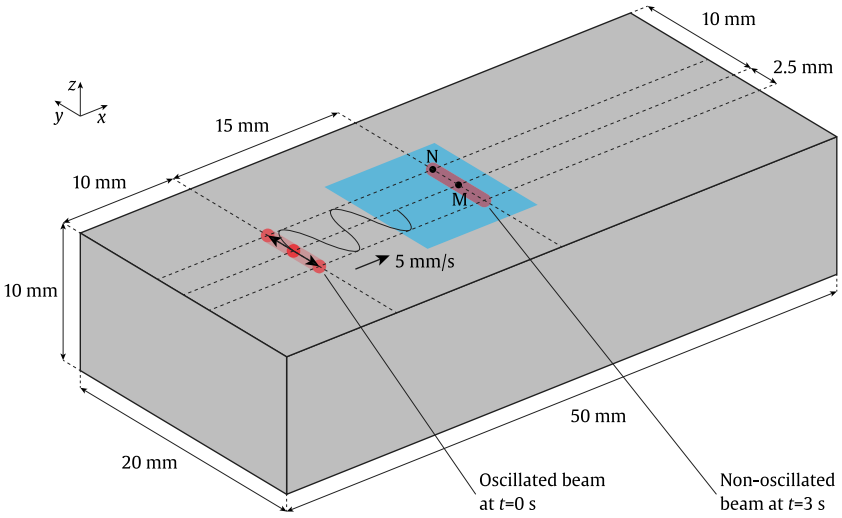

Fig. 1. Schematical overview of the substrate, the path (here sinusoidal) of the oscillated laser spot (at $t = 0$ s) and non-oscillated beam (at $t = 3$ s, so the beam has moved by 5 mm/s × 3 s = 15 mm). Locations M and N are used for temporal evaluations, the blue area indicates the location of the spatial evaluations, both at $t = 3$ s. (For interpretation of the references to color in this figure legend, the reader is referred to the web version of this article.)

profile is generally defined for a non-oscillated laser intensity profile. When employing a Galvanometer Scanner as beam shaping method, the above mentioned differences between the oscillated laser beam and the equivalent non-oscillated laser beam induced thermal cycles should be quantified as function of the oscillation frequency to determine which oscillation frequency is required to still obtain the desired peak temperatures and cooling rates.

In this work thermal models are developed to simulate the thermal fields induced by on the one hand the oscillated beams on the other hand the non-oscillated equivalent beam. Section 2 introduces these models and the evaluated areas and locations of interest. The thermal fields will be compared both spatially and temporally and discussed in Section 3. Finally, Section 4 summarizes the main conclusions of this work.

2. Method

To compare the thermal fields induced by the oscillated laser beams with those induced by the non-oscillated equivalent, thermal models have been developed in COMSOL Multiphysics® [16], as described in Section 2.1. The thermal models are subsequently solved and evaluated both temporally and spatially, and discussed in Section 2.2.

2.1. Model

In the model, the oscillated and non-oscillated equivalent laser beams are translated over a substrate with dimensions 50×20×10 mm^3, as schematically shown in Fig. 1. Stainless Steel 316L is chosen as the material of the substrate. In this model laser material process without melt is simulated, e.g. laser annealing or laser transformation hardening. Therefore phase transitions are not included in this and the material properties are fully described by its values for density ρ, thermal conductivity k, heat capacity C_p at constant pressure and absorption coefficient A. The density ρ reads

$$\rho = 8058.746 - 0.1963973\ T - 4.830884 \cdot 10^{-4}\ T^2 + 4.114383 \cdot 10^{-7}\ T^3 - 1.337946 \cdot 10^{-10}\ T^4 \quad \mathrm{kg/m^3}, \tag{1}$$

the thermal conductivity k reads

$$k = 7.956002 + 0.02084122\ T - 4.706772 \cdot 10^{-6}\ T^2 + 6.271478 \cdot 10^{-10}\ T^3 - 1.240772 \cdot 10^{-12}\ T^4 \quad \mathrm{W/mK} \tag{2}$$

and the heat capacity C_p at constant pressure reads

$$C_\mathrm{p} = 235.650788 + 1.30084242\ T - 0.00189052617\ T^2 + 1.34841366 \cdot 10^{-6}\ T^3 - 3.43379416 \cdot 10^{-10}\ T^4 \quad \mathrm{J/kgK}, \tag{3}$$

which all are temperature dependent and retrieved from the COMSOL Multiphysics® material library [16].

The absorbed laser energy is assumed to be converted into heat instantly in an infinitely small surface layer, with an absorption coefficient of $A = 0.3$ (for laser wavelengths around 1 μm) [17].

Both the oscillated and stationary heat sources start at location $x_0 = 10$ mm and $y_0 = 10$ mm and are translated over the surface of the substrate in positive x-direction at a traverse velocity $v = 5$ mm/s. The following sections define the oscillated and stationary heat sources in more detail.

2.1.1. Scanned laser beam

It is assumed that the focal spot of the laser beam shows a top-hat laser intensity distribution, defined as

$$I_\mathrm{U}(x,y,t) = \begin{cases} \frac{P(t)}{\pi r_\mathrm{f}^2} & , x^2 + y^2 \le r_\mathrm{f}^2, \\ 0 & , x^2 + y^2 > r_\mathrm{f}^2, \end{cases} \tag{4}$$

where $P(t)$ is the laser power and $r_\mathrm{f} = 0.5$ mm the radius of the focal spot. This laser spot is oscillated over the substrate along a path described by

$$\begin{Bmatrix} x_\mathrm{s}(t) \\ y_\mathrm{s}(t) \end{Bmatrix} = \begin{Bmatrix} 0 \\ a \sin(2\pi f_y t) \end{Bmatrix}, \tag{5}$$

where $a = 2.5$ mm is the amplitude and f_y the oscillation frequency of the path. The studied oscillation frequencies f_y are 5, 10, 20, 50, 100 and 200 Hz. To avoid high intensities at the turning points of the sinusoidal trajectory, the laser power is scaled along the path as

$$P(t) = \bar{P}\frac{\pi}{2}|\cos 2\pi f_y t|, \tag{6}$$

where $\bar{P} = 500$ W is the average laser power. Then the heat input in the model is defined as

$$q_\mathrm{in} = A I_\mathrm{U}(x - x_\mathrm{s}(t) - vt - x_0, y - y_\mathrm{s}(t) - y_0, t). \tag{7}$$

2.1.2. Non-oscillated equivalent laser beam

The non-oscillated laser intensity profile corresponding to (or equivalent to) a spot oscillating in y-direction can be derived using [18]

$$I_\mathrm{S}(x,y) = I_\mathrm{U}(x,y) * S(x,y)$$

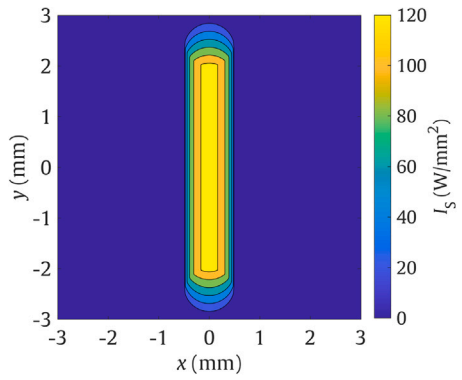

Fig. 2. Laser intensity profile I_S of non-oscillated equivalent beam.

$$= \iint_{A_S} I_U(x-x', y-y')S(x', y')dx'dy', \tag{8}$$

which is the mathematical convolution between the unshaped laser intensity (Eq. (4)) profile of the focal spot and the so-called shape function S

$$S(x,y) = \frac{1}{T\bar{P}} \int_0^T \delta(x - x_s(t))\delta(y - y_s(t))P(t)dt, \tag{9}$$

as function of the oscillation trajectory (Eq. (5)) and the power history (Eq. (6)). More details about this procedure can be found in our earlier work [18]. By applying Eqs. (8) and (9) to Eqs. (4), (5) and (6) the shaped laser intensity profile is obtained as

$$I_S(x,y) = \begin{cases} \frac{\bar{P}\sqrt{r_f^2 - x^2}}{\pi r_f^2 a}, & |x| \le r_f, |y| \le a - \sqrt{r_f^2 - x^2} \\ \frac{\bar{P}\left(\sqrt{r_f^2 - x^2} + a - |y|\right)}{2\pi r_f^2 a}, & |x| \le r_f, a - \sqrt{r_f^2 - x^2} < |y| \le a + \sqrt{r_f^2 - x^2}, \end{cases} \tag{10}$$

The corresponding applied heat input in the model for this laser beam equals

$$q_{in} = AI_S(x - vt - x_0, y - y_0). \tag{11}$$

Fig. 2 shows this equivalent non-oscillated intensity profile.

2.2. Evaluation

The obtained thermal fields are evaluated both temporally and spatially. At two locations the thermal cycle is evaluated, i.e. locations M and N in Fig. 1. The laser beam passes these locations at $t = 3$ s, so $x_M = x_N = 25$ mm. Location M is located at the center of the oscillation line at $y_M = 10$ mm and location N at one of the turning points of the oscillation path, so $y_N = 12.5$ mm.

Differences in these thermal cycles will be induced by different irradiation cycles. The non-oscillated beam will pass location M once while traveling in x-direction. Therefore, the non-oscillated beam will irradiate location M only once, with a relatively low intensity for a relatively long period. This irradiation cycle is shown in blue in Fig. 3(a). For the oscillated beams, location M is passed at a frequency of two times the oscillation frequency (because location M is passed two times per period). As can be observed from this figure, in location M the irradiation time per pass decreases with increasing oscillation frequencies. Fig. 3(b) shows the irradiation cycles of location N. Here the non-oscillated irradiation intensity is half of that of location M according to Eq. (10). As location N is located at the turning points of the sinusoidal oscillation path, the location is irradiated only once per period. As can be observed from the figure the irradiation durations are longer compared to the irradiation durations of location M. The dips

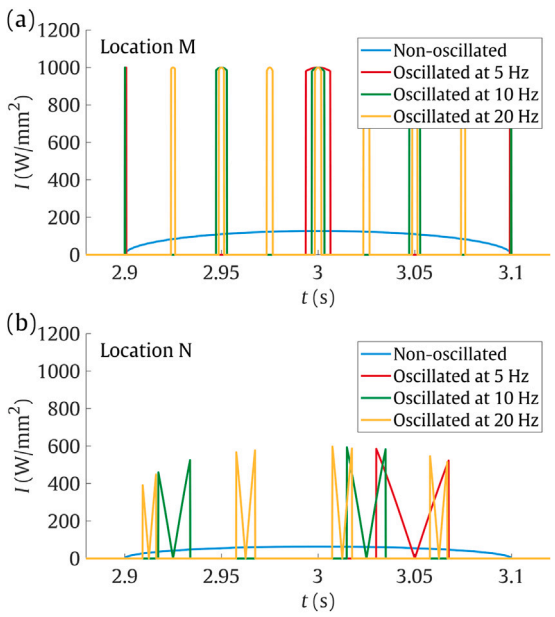

Fig. 3. Irradiation cycles by non-oscillated and oscillated beams of (a) location M and (b) location N at oscillation frequencies of 5, 10 and 20 Hz.

in the irradiation during the passes is caused by the power reduction at the turning points, as defined in Eq. (6).

The analysis of the laser-induced temperature profiles is studied in the area enclosed by lines at $x = 17.5$ mm, $x = 27.5$ mm, $y = 5$ mm and $y = 15$ mm, as indicated by the blue area in Fig. 1. The temperature and cooling rate fields of the indicated area will be studied at $t = 3$ s.

3. Results and discussion

Fig. 4(a) shows the thermal cycles at location M induced by oscillated beams at oscillation frequencies f_y of 5, 10 and 20 Hz as well as the non-oscillated equivalent laser intensity distribution (blue curve). It can be observed from this figure that the non-oscillated beam induces a relatively slow heating and cooling of the material when passing location M, with a maximum around $T = 1400$ K. For the oscillated beams, the multiple beam passes with high(er) intensity induce multiple rapid heating and cooling cycles, resulting in a temperature cycle oscillating around the temperature profile induced by the non-oscillated beam. Please note that these thermal profiles exceed the melting point of the stainless steel (≈1650 K), which is undesired. As phase transformations are not modeled this will lead to lower peak temperatures in practice. The deviations in temperature induced by the oscillated beams relative to the temperature cycle induced by the non-oscillated one are shown in Fig. 4(b). From this figure, it can be observed that for increasing oscillation frequencies the maximum temperature deviation is decreasing. More specifically, a quadrupling of the oscillation frequency (from 5 to 20 Hz) leads to halving of the maximum deviation. The latter are similar trends as found during laser transformation hardening in the work of Soriano et al. [19].

The thermal cycles induced by the (non-)oscillated beams at location N are shown in Fig. 4(c). For the non-oscillated beam (blue curve) the thermal cycle is similar to the cycle at location M, only with a lower peak temperature. The thermal cycles induced by the oscillated beams are again oscillating around the cycle induced by the non-oscillated beam, the deviations with respect to this thermal cycle are shown in Fig. 4(d). This figure shows longer durations of overheating at a lower frequency compared to the results at location M (Fig. 4(b)). Also, double temperature peaks can be observed. This lower frequency is caused by less passes of the laser beam at location N as compared to

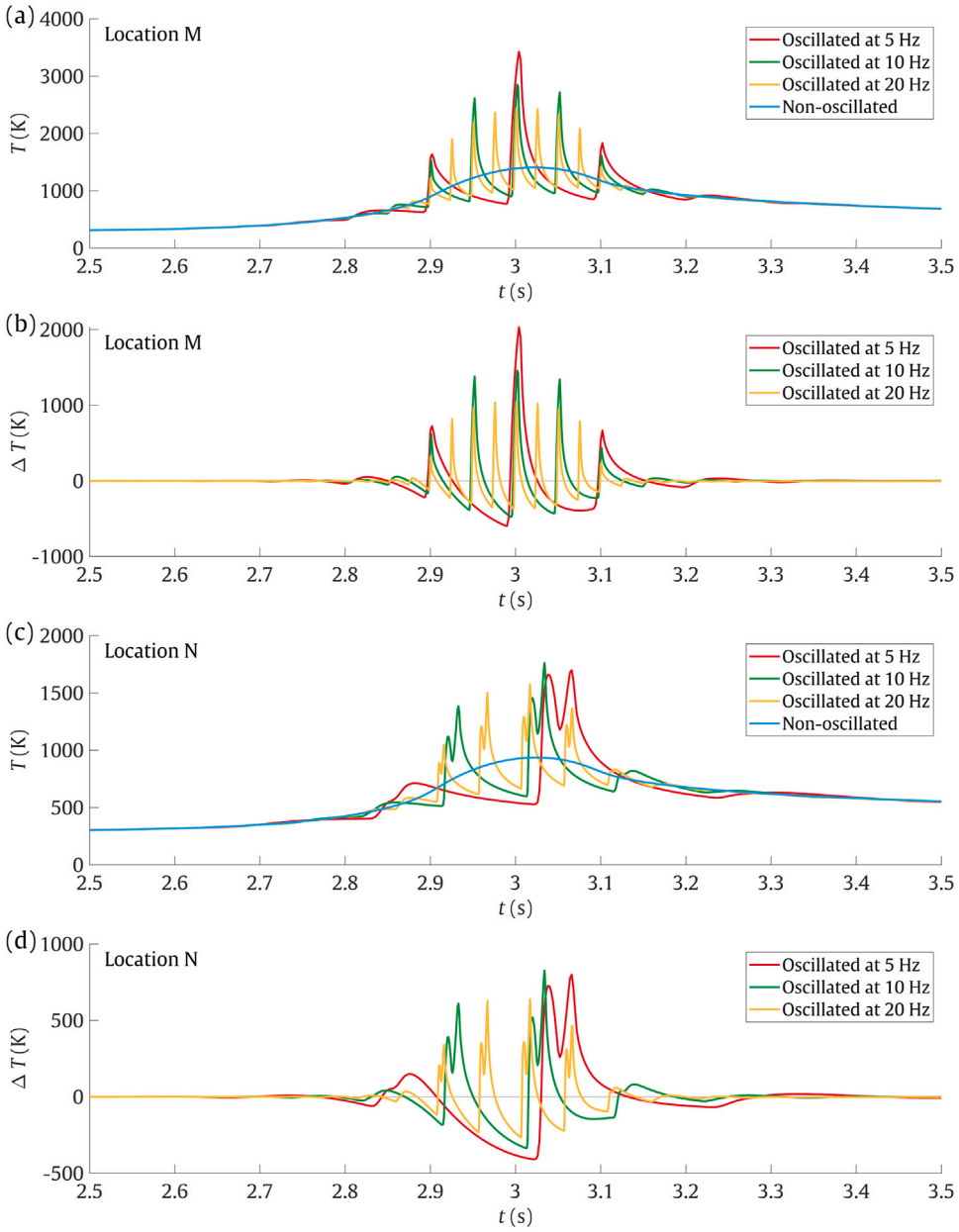

Fig. 4. (a), (c) Thermal cycles induced by non-oscillated and oscillated laser beam intensity profiles (b), (d) difference between thermal cycles induced by the oscillated beams and thermal cycle induced by the non-oscillated beam for (a), (b) location M and (c), (d) location N at oscillation frequencies of 5, 10 and 20 Hz.

location M, as explained in Section 2.2 and visualized in Fig. 3. The longer durations of overheating with the double peaks are a result of the temporal shape of the irradiation cycles, which can also be observed in Fig. 3(b).

To illustrate the effect of further increasing the oscillation frequency, Figs. 5(a) and (c) show the induced thermal cycles by the beams oscillated at oscillation frequencies f_y of 50, 100 and 200 Hz and the non-oscillated beam at respectively locations M and N. The deviations of the thermal profiles induced by the oscillated beams with respect to the thermal profile induced by the non-oscillated ones are shown in Figs. 5(b) and (d). It can be observed that the maximum positive deviations are much larger than the maximum negative deviations, ranging from approximately a factor 3 at location M in Fig. 5(b) to a factor 2 at location N in Fig. 5(d).

Like was found for the lower oscillation frequencies, also for these higher oscillation frequencies the maximum deviation is halved by a quadrupling of the oscillation frequency. Therefore the lowest maximum temperature deviation, which is still around 325 K, is found at the highest oscillation frequency of 200 Hz. This can also be observed from Fig. 6, where the maximum positive and negative deviations (i.e. overheating and underheating) at both locations for the different frequencies are plotted in a log–log plot. The dots in this plot represent the simulation data at the different frequencies. The lines shown in the graph are characterized by a slope of −0.5 on logarithmic scale. Using the average of the data points for the frequencies of 50, 100 and 200 Hz the vertical position of the lines were constructed. This linear relation on log–log scale, between oscillation frequency f_y and temperature deviations $\Delta T_{\max}$ is similar to the temperature difference induced by a pulsed laser source as function of varying pulse durations. More specifically, in the case of a pulsed laser, the temperature difference scales with the square root of the pulse duration, as was derived analytically by Belchtel in 1975 [20]. As in the oscillated case considered in this

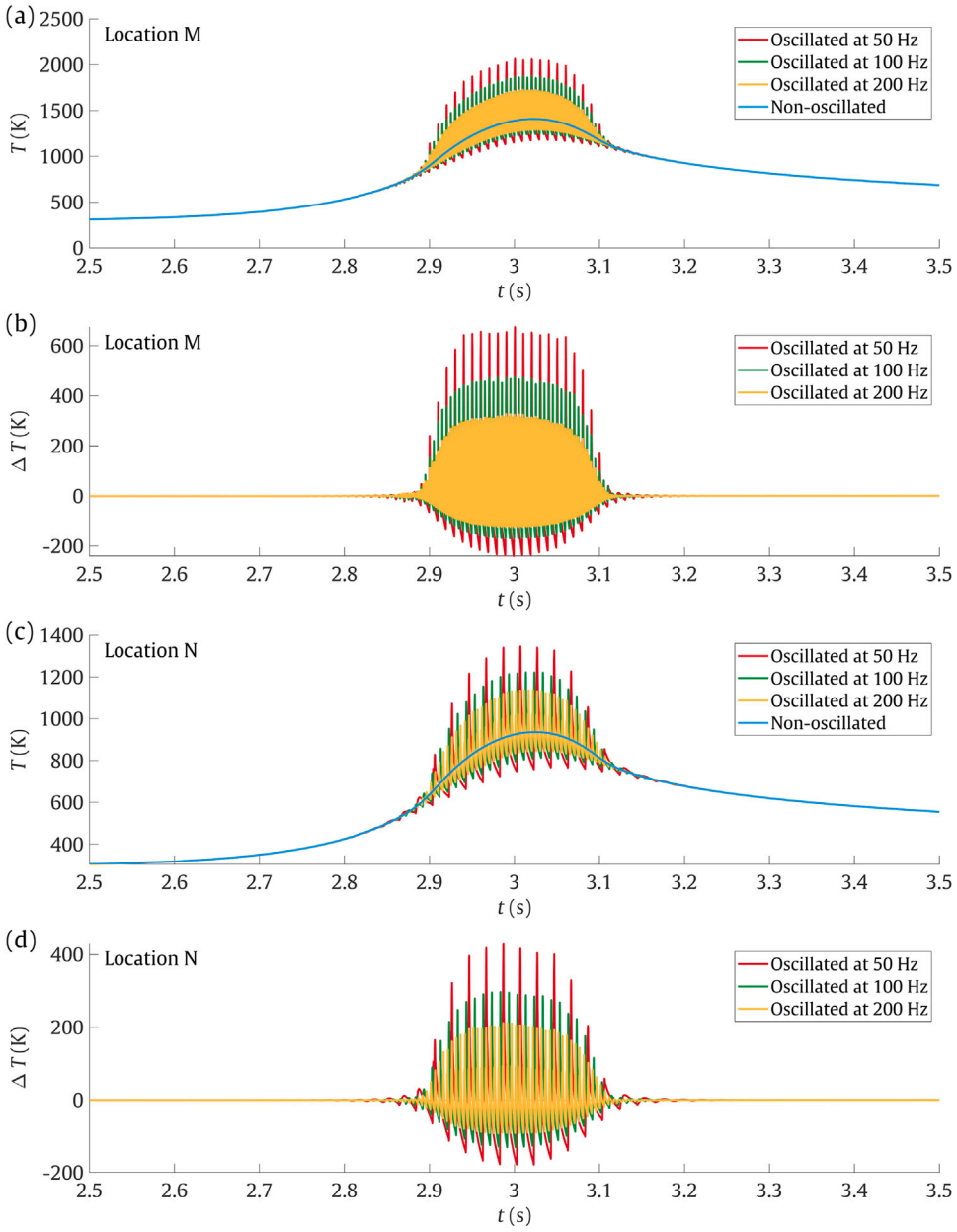

Fig. 5. (a), (c) Thermal cycles induced by non-oscillated and oscillated laser beam intensity profiles (b), (d) difference between thermal cycles induced by the oscillated beams and thermal cycle induced by the non-oscillated beam for (a), (b) location M and (c), (d) location N at oscillation frequencies of 50, 100 and 200 Hz.

paper, the irradiations cycles (in Fig. 3) are in fact to be considered to be laser pulses. The pulse duration of these pulses is inversely proportional to the oscillation frequency. From this it follows that, indeed, in the case of a oscillated beam the temperature difference is inversely proportional to the square root of the oscillation frequency. As can be concluded from Fig. 6, some of the data points corresponding to low oscillation frequencies deviate from the linear trend. This is attributed to the fact that the effect of the traverse velocity v becomes significant at low oscillation frequencies, e.g. location N is only irradiated by the side of the oscillated laser beams at low oscillation frequencies. From the above analysis a design rule can be derived, namely in the case a reduction of temperature deviations of a factor of two is targeted, the oscillation frequency should be quadrupled.

The thermal profiles on the surface of the substrate induced by both beam types at time $t = 3$ s are shown in Fig. 7. Fig. 7(a) shows the thermal profile induced by the non-oscillated equivalent beam. This temperature profile is characterized by a line shaped high temperature zone, with slightly increasing temperatures towards the center of the line. In Fig. 7(b) the thermal profile is presented that is induced by the oscillated laser beam profile at 200 Hz. This oscillation frequency induces a thermal profile closest to the one induced by the non-oscillated beam. The temperature profile in Fig. 7(b) shows a zone with high temperatures clearly marking the current position of the laser focal spot. Furthermore the oscillation direction of the focal spot, in positive y-direction, can be deduced from the higher temperatures in the just irradiated areas ($24.5 < x < 25.5$ mm and $7.5 < y < 10$ mm). These areas show higher temperatures compared to the thermal field induced by the non-oscillated beam (Fig. 7(a)), whereas the areas that are about to be irradiated show lower temperatures compared to that field. This implies that the oscillated beam induces large temperature differences in short times and therefore implying high heating and cooling rates of the substrate. The induced cooling rates, for both the non-oscillated and oscillated cases, are shown in Fig. 8. It can be observed the oscillated beam case (Fig. 8(b)) results indeed in much higher cooling

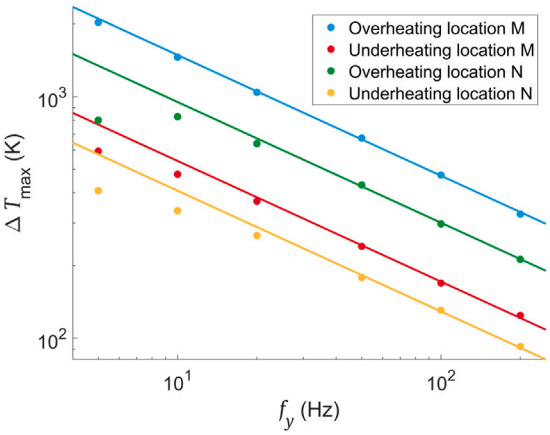

Fig. 6. Maximum differences between thermal cycles induced by the oscillated beams and thermal cycle induced by the non-oscillated beam as function of oscillation frequency.

rates compared to the non-oscillated case (Fig. 8(a)). For example, if the cooling rate at a local temperature of 1200 K is relevant for the laser material process, the non-oscillated case results in a maximum cooling rate around 5500 K/s at this temperature, whereas the oscillated case gives significantly larger cooling rates, which are over 10^5 K/s at this temperature. Hence, beam shaping based on the oscillation method results in significantly different thermal fields and cooling rates compared to shaping the beam in a non-oscillated approach. As these quantities are important factors in the resulting microstructure for multiple high power laser processes [21], these different beam shaping methods may also induce different microstructures.

4. Conclusion

The thermal fields and cycles, induced by both oscillated laser beam intensity profiles and its non-oscillated equivalent laser beam intensity profile are simulated using a thermal model. The obtained thermal profiles induced by the oscillated intensity profiles are, both spatially and temporally, compared to the thermal results induced by the non-oscillated equivalent profile. From the thermal cycles at two locations induced by the oscillated beams and the non-oscillated equivalent beam, it was concluded that the temperature differences decrease by a factor 2 when the oscillation frequency is increased by a factor 4, following the analytical solution. This is a design rule which can be exploited to optimize the processing result. Also the cooling rates induced by the oscillated beam profiles are much higher than the cooling rates induced by the non-oscillated equivalent beam. For the whole area illuminated by the oscillated beam profile during one cycle, the cooling rates are two orders of magnitude larger than the cooling rates obtained by the non-oscillated beam profile. These are a result of the fast thermal cycles induced by oscillated beams compared to a single slow thermal cycle induced by the non-oscillated equivalent beam. From above observations it can be concluded that even for a oscillation frequency of 200 Hz, from a thermal point of view, the differences between the thermal profiles and cycles induced by the oscillated laser intensity profile and the thermal profiles and cycles induced by the non-oscillated equivalent laser intensity profile are significant. This means that when the Galvanometer Scanner is used to obtain a desired beam shape, the obtained processing results, such as microstructures or residual stress distributions, probably will differ from the results obtained using a non-oscillating beam shaping method.

CRediT authorship contribution statement

Scholte J.L. Bremer: Writing – review & editing, Writing – original draft, Visualization, Validation, Software, Resources, Project administration, Methodology, Investigation, Formal analysis, Data curation, Conceptualization. **Ronald G.K.M. Aarts:** Writing – review & editing, Supervision. **Gert-willem R.B.E. Römer:** Writing – review & editing, Supervision, Funding acquisition, Conceptualization, Project administration.

Declaration of competing interest

The authors declare that they have no known competing financial interests or personal relationships that could have appeared to influence the work reported in this paper.

Data availability

Data will be made available on request.

Acknowledgments

This research was carried out under project number P16-46/S17024m, which is part of AiM2XL program (www.m2i.nl/aim2xl/), in the framework of the Partnership Program of the Materials innovation institute M2i (www.m2i.nl) and the Netherlands Organization for Scientific Research (www.nwo.nl). The research was conducted in collaboration with industrial partners and supported by the Rotterdam Fieldlab Additive Manufacturing BV (RAMLAB), www.ramlab.com.

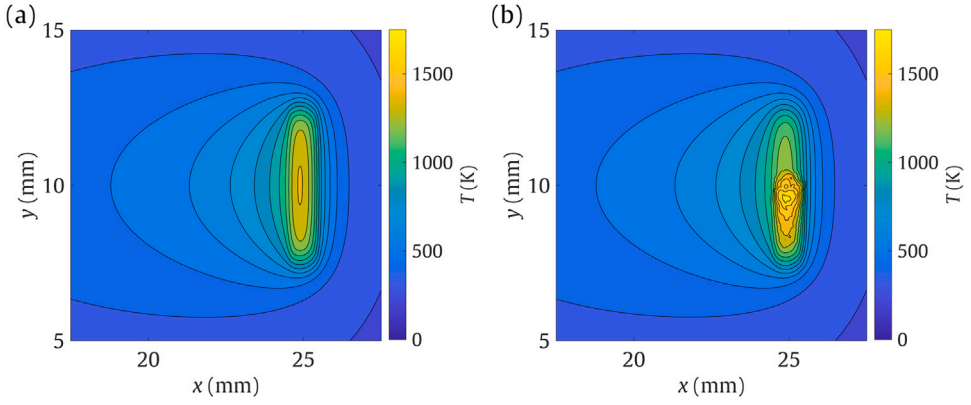

Fig. 7. Temperature profile at $t = 3$ s induced by (a) non-oscillated equivalent laser beam profile and (b) oscillated laser beam profile at 200 Hz.

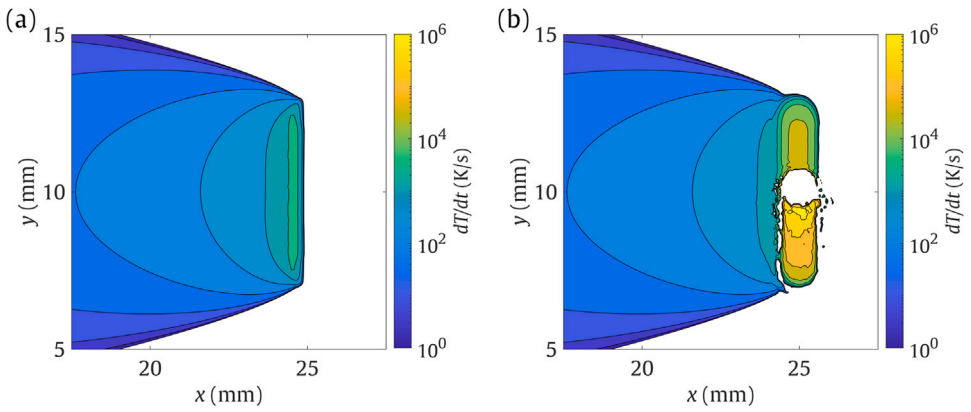

Fig. 8. Cooling rates at $t = 3$ s induced by (a) non-oscillated equivalent laser beam profile and (b) oscillated laser beam profile at 200 Hz.

References

[1] H.S. Dewi, A. Fischer, J. Volpp, T. Niendorf, A.F.H. Kaplan, Microstructure and mechanical properties of laser surface treated 44MnSiVS6 microalloyed steel, Opt. Laser Technol. 127 (2020) 106139, http://dx.doi.org/10.1016/j.optlastec.2020.106139.

[2] F. Klocke, M. Schulz, S. Gräfe, Optimization of the laser hardening process by adapting the intensity distribution to generate a top-hat temperature distribution using freeform optics, Coatings 7 (6) (2017) 77, http://dx.doi.org/10.3390/coatings7060077.

[3] D. Wellburn, S. Shang, S.Y. Wang, Y.Z. Sun, J. Cheng, J. Liang, C.S. Liu, Variable beam intensity profile shaping for layer uniformity control in laser hardening applications, Int. J. Heat Mass Transfer 79 (2014) 189–200, http://dx.doi.org/10.1016/J.IJHEATMASSTRANSFER.2014.08.020.

[4] M. Rasch, C. Roider, S. Kohl, J. Strauß, N. Maurer, K.Y. Nagulin, M. Schmidt, Shaped laser beam profiles for heat conduction welding of aluminium-copper alloys, Opt. Lasers Eng. 115 (2019) 179–189, http://dx.doi.org/10.1016/J.OPTLASENG.2018.11.025.

[5] C. Prieto, E. Vaamonde, D. Diego-Vallejo, J. Jimenez, B. Urbach, Y. Vidne, E. Shekel, Dynamic laser beam shaping for laser aluminium welding in e-mobility applications, Procedia CIRP 94 (2020) 596–600, http://dx.doi.org/10.1016/j.procir.2020.09.084.

[6] Y. Mi, P. Guglielmi, M. Nilsen, F. Sikström, G. Palumbo, A. Ancona, Beam shaping with a deformable mirror for gap bridging in autogenous laser butt welding, Opt. Lasers Eng. 169 (2023) 107724, http://dx.doi.org/10.1016/j.optlaseng.2023.107724.

[7] S. Shang, D. Wellburn, Y. Sun, S. Wang, J. Cheng, J. Liang, C. Liu, Laser beam profile modulation for microstructure control in laser cladding of an NiCrBSi alloy, Surf. Coat. Technol. 248 (2014) 46–53, http://dx.doi.org/10.1016/J.SURFCOAT.2014.03.018.

[8] T.T. Roehling, S.S.Q. Wu, S.A. Khairallah, J.D. Roehling, S.S. Soezeri, M.F. Crumb, M.J. Matthews, Modulating laser intensity profile ellipticity for microstructural control during metal additive manufacturing, Acta Mater. 128 (2017) 197–206, http://dx.doi.org/10.1016/j.actamat.2017.02.025.

[9] S.J.L. Bremer, M. Luckabauer, G.R.B.E. Römer, Laser intensity profile as a means to steer microstructure of deposited tracks in Directed Energy Deposition, Mater. Des. 227 (2023) 111725, http://dx.doi.org/10.1016/J.MATDES.2023.111725.

[10] S. Feuchtenbeiner, T. Hesse, N. Speker, P. Haug, J. Seebach, W. Dubitzky, D. Havrilla, J.-P. Hermani, Beam shaping BrightLine Weld: latest application results, in: S. Kaierle, S.W. Heinemann (Eds.), High-Power Laser Materials Processing: Applications, Diagnostics, and Systems VIII, Vol. 10911, SPIE, 2019, p. 109110X, http://dx.doi.org/10.1117/12.2509560.

[11] N.J. Goffin, R.L. Higginson, J.R. Tyrer, The use of holographic optical elements (HOE's) to investigate the use of a flat irradiance profile in the control of heat absorption in wire-fed laser cladding, J. Mater. Process. Technol. 220 (2015) 191–201, http://dx.doi.org/10.1016/j.jmatprotec.2015.01.023.

[12] P. Sancho, F. Cordovilla, J. Dominguez, M.Á. Montealegre, J. Isaza, Á. García-Beltrán, J.L. Ocaña, Customized laser beam intensity distribution for the laser surface treatment of geometrically convoluted components, J. Mater. Process. Technol. 263 (2019) 223–232, http://dx.doi.org/10.1016/J.JMATPROTEC.2018.08.020.

[13] P. Horník, H. Šebestová, J. Novotný, L. Mrňa, Laser beam oscillation strategy for weld geometry variation, J. Manuf. Process. 84 (2022) 216–222, http://dx.doi.org/10.1016/J.JMAPRO.2022.10.016.

[14] M. Meunier, A. Kumar, A. Lucas, S. Bernard, R. Arias, J.L. Arias Otero, G. Pallier, G. Labroille, Stainless steel laser beam welding with a dynamic tailored beam shaping laser-head based on multi-plane light conversion, in: LiM 2023 Proceedings, 2023, http://dx.doi.org/10.1117/12.2655458.

[15] E. Shekel, Y. Vidne, B. Urbach, 16kW single mode CW laser with dynamic beam for material processing, in: L. Dong, M.N. Zervas (Eds.), Fiber Lasers XVII: Technology and Systems, Vol. 11260, SPIE, 2020, 1126021, http://dx.doi.org/10.1117/12.2545900.

[16] COMSOL Multiphysics® v. 5.5, COMSOL AB, Stockholm, Sweden.

[17] W.M. Steen, J. Mazumder, Basic laser optics, in: Laser Material Processing, fourth ed., Springer, London, United Kingdom, 2010, pp. 79–130, http://dx.doi.org/10.1007/978-1-84996-062-5_3.

[18] S.J.L. Bremer, R.G.K.M. Aarts, G.R.B.E. Römer, Mathematical analysis of dynamic high power laser beam shaping using Galvanometer Scanners or Deformable Mirrors, 2023, http://dx.doi.org/10.2139/ssrn.4595382, SSRN.

[19] C. Soriano, G. Alberdi, J. Lambarri, A. Aranzabe, A.J. Yáñez, Study of the influence of the oscillation frequency on the surface hardening process of the 42CrMo4 alloy using an oscillating laser beam, Surf. Coat. Technol. 409 (2021) 126877, http://dx.doi.org/10.1016/j.surfcoat.2021.126877.

[20] J.H. Bechtel, Heating of solid targets with laser pulses, J. Appl. Phys. 46 (4) (1975) 1585–1593, http://dx.doi.org/10.1063/1.321760.

[21] J.C. Ion, Engineering Materials, in: J.C. Ion (Ed.), Laser Processing of Engineering Materials, first ed., Butterworth-Heinemann, Oxford, United Kingdom, 2005, pp. 139–177, http://dx.doi.org/10.1016/B978-075066079-2/50008-8.